High-performance transparent thin-film transistor based on Y_2O_3/In_2O_3 with low interface traps

H. Z. Zhang, L. Y. Liang, A. H. Chen, Z. M. Liu, Z. Yu, H. T. Cao,[a] and Q. Wan[b]
Ningbo Institute of Materials Technology and Engineering (NIMTE), Chinese Academy of Sciences (CAS), Ningbo 315201, People's Republic of China

(Received 2 June 2010; accepted 2 September 2010; published online 24 September 2010)

High-performance Y_2O_3/In_2O_3-based transparent thin-film transistors were processed featuring low thermal budget. The device shows a field-effect mobility of 43.5 $cm^2 V^{-1} s^{-1}$, a subthreshold swing of 0.28 V/decade, and an on/off current ratio of 10^8. These results are attributed to the high dielectric constant of Y_2O_3 and unique electronic structure of In_2O_3. Furthermore, the cubic phases of crystalline Y_2O_3 and In_2O_3 films have the identical crystal structure with a small lattice mismatch, which provides a well-defined dielectric/semiconductor interface for the optimal performance. © *2010 American Institute of Physics*. [doi:10.1063/1.3492852]

Transparent oxide semiconductor (TOS)-based thin-film transistors (TTFTs) used as pixel driver backplanes in the active-matrix liquid crystal displays have attracted considerable attention.[1,2] The explored semiconductor materials are focused on ZnO, In_2O_3, In–Zn–O (IZO), In–Ga–Zn–O (IGZO),[3–9] involving a class of binary, ternary, and quaternary TOSs. The main advantages of TOSs used as active layers include high field effect mobility, good transparency in the visible spectral region, and low processing temperature. In_2O_3 is one of the representative TOS materials. In particular, the bottom of the conduction band of In_2O_3 mainly consists of single free electronlike band of In 5*s* states,[10] while the valence band edge arises from the O 2*p* states hybridized with In 4*d* states.[11] This unique band structure essentially results in uniform distribution of the charges that reduces the scattering to a minimum, which makes In_2O_3 appealing in carrier mobility.

Apart from the active layer, the gate dielectric is also of great importance for the fabrication of high-performance TTFTs. Among the high dielectric constant materials, Y_2O_3 has been regarded as one of good insulators as a consequence of its desirable physical properties such as wide band gap (5.5–6 eV), relatively high dielectric constant (14–18).[12–15] A wide band gap can enlarge the conduction band offset between the gate dielectric and active layer so as to suppress the leakage current, while a high dielectric constant can yield a small subthreshold swing (*SS*) and low threshold voltage (V_{th}).[16] The conduction band offset (ΔE_C) between the dielectric Y_2O_3 and the active layer In_2O_3 is about 2.6 eV (nearly equal to 30 000 K),[17] which is sufficient to block leakage current. Especially, crystalline Y_2O_3 and In_2O_3 have the same cubic bixbyte structure, which is favorable to obtain abrupt and clean interfaces (just like the case of heteroepitaxial growth). As we know in transistors, charge accumulation and transport occur close to the interface between insulator and semiconductor (I/S), implying that a well-matched interface in favor of mitigating electron trapping is fundamental for the transistor performance.

In this work, we report high-performance TTFTs prepared on ITO glasses using crystalline In_2O_3 and Y_2O_3 thin films as channels and dielectrics, respectively. It is noteworthy that, all the layers in our device were deposited by magnetron sputtering without using the substrate heater, and no postannealing treatment was applied as well.

Y_2O_3 thin films were deposited by reactive rf magnetron sputtering with an input power of 100 W by using a commercially available 2 in. yttrium metallic target (4N) under an optimum Ar/O_2 gas flow rate ratio of 4.5 SCCM/0.5 SCCM (SCCM denotes cubic centimeter per minute at STP) and a total working pressure of 0.19 Pa. In_2O_3 thin films were prepared by rf magnetron sputtering from a 2 in. In_2O_3 ceramic target (4N) with a power of 100 W. The optimum preparation parameters for In_2O_3 are an Ar/O_2 gas flow rate ratio of 6 SCCM/6 SCCM, a total working pressure of 0.55 Pa, and a film thickness of 60 nm. The channel layers have a relatively low electron density ($\sim 1.2 \times 10^{16}$ cm^{-3}) according to Hall effect measurement (ACCENT, HL5500). IZO amorphous thin films (170 nm) with metal-like conductivity were used as source/drain (S/D) electrode.[18] The film structures were examined using a Bruker D8 x-ray diffractometer. The optical properties of Y_2O_3 thin films were measured via a variable angle spectroscopic ellipsometer (J.A.Woollam Co., Inc.) in the UV-vis-NIR range. X-ray photoelectron spectroscopy (XPS, Kratos Analytical Ltd., U.K.) was used to analyze the binding structure of the yttria films.

The schematic of the In_2O_3-TTFT is shown in the inset of Fig. 1. The pattern was defined by a shadow mask on the semiconductor layer with a channel length (L) of 100 μm and a channel width (W) of 400 μm. The entire device features a good transparency with an average transmittance over 80% in the visible spectral region (Fig. 1), which is requisite to enlarge the aperture ratio of pixel and develop see-through displays.

Figure 2(a) shows x-ray diffraction (XRD) patterns of the Y_2O_3 film on ITO glass substrate. There are four diffraction peaks which correspond to cubic (*Ia*3 space group, Joint Committee on Powder Diffraction Standards (JCPDS) card 25–1200) and monoclinic ($C2/m$ space group, JCPDS card 44–0399) phases of Y_2O_3, revealing that the dominated cubic phase is mixed with the monoclinic one. As depicted in Fig. 2(b), the In_2O_3 film only shows the cubic structure (*Ia*3 space group, JCPDS card 06–0416). The cubic phases of Y_2O_3 and In_2O_3 have the identical crystal structure with a

[a]Electronic mail: h_cao@nimte.ac.cn.
[b]Electronic mail: wanqing@nimte.ac.cn.

0003-6951/2010/97(12)/122108/3/$30.00 © 2010 American Institute of Physics

Downloaded 26 Sep 2010 to 130.237.29.138. Redistribution subject to AIP license or copyright; see http://apl.aip.org/about/rights_and_permissions

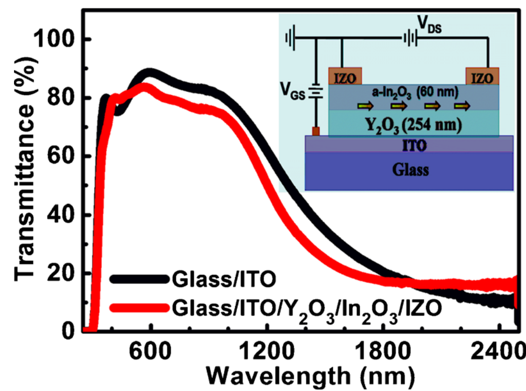

FIG. 1. (Color online) The optical transmission spectrum for the entire device and ITO glass. The inset is the cross-sectional schematic of the studied device.

small lattice mismatch (roughly 5.1% in this study), which could result in abrupt and clean interfaces with low electron traps.

The thickness, refractive index (n) and extinction coefficient (k) of Y_2O_3 thin films were obtained by fitting the ellipsometry spectra in the wavelength (λ) range of 190–1700 nm. The optical band gap (E_g) of the films was extracted by extrapolating the linear portion of the $(\alpha h\nu)^2$ versus photon energy ($h\nu$) plot [Fig. 3(a)] to zero, where α is the absorption coefficient which can be obtained via $\alpha=4\pi k/\lambda$. The n spectrum is also displayed in the inset of Fig. 3(a). The thickness, E_g, and n (@543 nm) are 254 nm, 6.0 eV, and 1.844, respectively. The optical band gap of the film is comparable to the literature (5.5–6.0 eV).[12,13] The n value (@534 nm) of Y_2O_3 films prepared at low temperatures ($\leq$300 °C) is between 1.7 and 1.8,[19,20] a little smaller than 1.844 in our case, implying that fewer voids were incorporated in our films since the refractive index is well correlated with the packing density of the film.[21]

XPS spectra of Y_2O_3 thin films are depicted in Fig. 3(b). The binding energy of Y $3d_{5/2}$ and $3d_{3/2}$ for the freshly etched surface located at 156.6 eV and 158.6 eV, respectively, which are consistent with the Ref. 22. There are no metallic Y related peaks present. The O 1s binding energy of the etched Y_2O_3 surface located at 529.1 eV [inset to Fig. 3(b)], corresponding to the O–Y bond, indicating the absence of physisorbed oxygen (531.3 eV).[23,24]

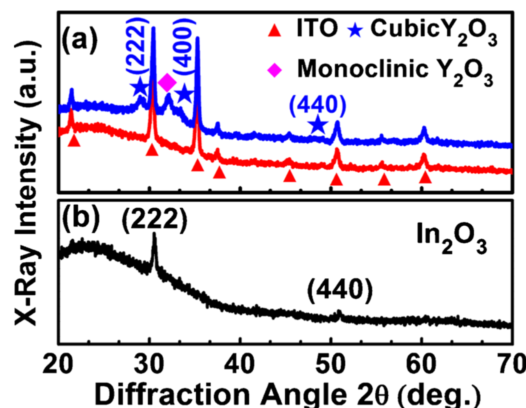

FIG. 2. (Color online) XRD patterns of (a) the fabricated Y_2O_3 film, ITO substrate and (b) the In_2O_3 film on glass slide.

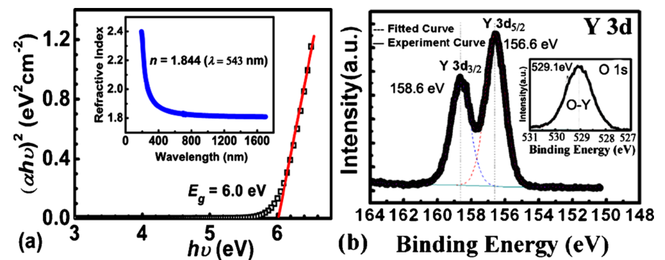

FIG. 3. (Color online) (a) Tauc plot for determining the optical band gap E_g of Y_2O_3 thin film, and the inset shows the refractive index as a function of wavelength λ. (b) Y $3d$ XPS spectrum of etched Y_2O_3 thin film, and the inset presents O 1s spectrum of etched Y_2O_3 thin film.

The dielectric properties were evaluated using an ITO/Y_2O_3/Cu capacitor, in which the ITO and Cu films were used as the bottom and top electrodes, respectively. The leakage current density versus electric field (J-E) of Y_2O_3 thin film is presented in Fig. 4(a), with a leakage current density of $\sim 4.4\times10^{-8}$ A/cm^2 at 1 MV/cm. The capacitances, measured with an inductance-capacitance-resistance meter at 1 MHz and 1 KHz, are around 52.4 nF/cm^2 and 59.0 nF/cm^2, respectively, as displayed in Fig. 4(b). The relative dielectric constant (ε) of Y_2O_3 thin film is about 15 (1 MHz), in good agreement with that of bulk Y_2O_3,[13–15] exhibiting as expected dielectric properties. From the above-mentioned optical, electrical, and compositional properties analysis, the Y_2O_3 thin films presented trade-off figures of merit between leakage and capacitance, which is crucial to decide how efficiently the gate voltage modulates the "off" to "on" current and how abruptly the device "turns on."

Figure 5 exhibits the output and transfer characteristics of In_2O_3-TTFT at a fixed V_{DS}=5 V. An obvious pinch-off voltage and current saturation are observed, with a high I_{DS} ($\sim$0.2 mA) at V_{GS}=10 V and V_{DS}=5 V. Also, the TTFT exhibits an on/off current ratio ($I_{\mathrm{on}}/I_{\mathrm{off}}$) of 10^8 and a low off-current of about 1.0×10^{-12} A, but it is not clear so far that the low off-current is mainly ascribed to the gate leakage or/and the current through the channel. For the practical high-resolution display applications, it is desirable to have a large on-current to drive pixels and a small off-current to lower power consumption. It is noteworthy that the turn-on voltage (V_{on}) is ~ -2 V, suggesting that the TTFT operated in depletion mode. Hence, there are accumulated mobile carriers in the In_2O_3 channel layer as shown in the band diagram, which is corresponding to the gray shadowed area in Fig. 5(b).

A saturation field-effect mobility (μ_{FE}) of 43.5 cm^2 V^{-1} s^{-1} and a threshold voltage (V_{th}) of 3.0 V were extracted from the slope and intercept of transfer character-

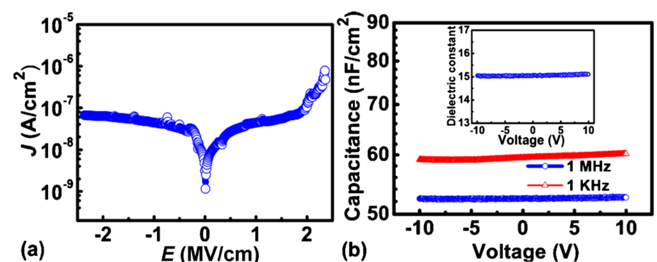

FIG. 4. (Color online) (a) Leakage current density and (b) C-V characteristics of Y_2O_3 thin film. The inset depicts the dielectric constant at 1 MHz.

Downloaded 26 Sep 2010 to 130.237.29.138. Redistribution subject to AIP license or copyright; see http://apl.aip.org/about/rights_and_permissions

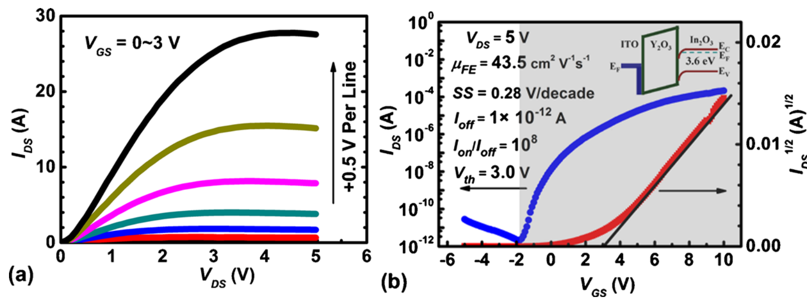

FIG. 5. (Color online) (a) The output characteristics and (b) transfer characteristics of the In_2O_3-TTFT. The inset is the energy band diagram for electron accumulation (the gray shadowed area).

istics of Fig. 4(b), respectively, using the following expression:

$$I_{DS} = \frac{WC_0\mu_{\mathrm{FE}}}{2L}(V_{GS} - V_{th})^2, \tag{1}$$

where C_0 is the capacitance per unit area of the gate dielectric. A low subthreshold swing (SS) of 0.28 V/decade was obtained by the maximum slope in the transfer curve. SS is related to the C_0 of the gate insulator material and the density of trap states N_{SS} at the I/S interface by the relation[25] $SS=(1/\log(e))(qN_{SS}/C_0+1)(k_BT/q)$, where k_B is Boltzmann's constant, T the temperature (in this case, 298 K), and q the electron charge. One can see that the low subthreshold swing can be attributed to both the high dielectric constant ε ($\varepsilon \propto C_0$) of Y_2O_3 and good quality of I/S interface with small N_{SS}, which were confirmed by the aforementioned results. Also, the well-defined I/S interface would benefit the μ_{FE} of the TTFT due to weakened interface scattering.

In summary, we have demonstrated high-performance In_2O_3-TTFTs with Y_2O_3 as the gate dielectrics. Due to the same cubic bixbyte structure of them, the good interface matching would lead to low interface traps. We shed light on the fundamental aspects of the Y_2O_3/In_2O_3 based TTFTs that the high device performance is linked to the good dielectric properties of Y_2O_3, the essential electronic structure of In_2O_3, and the well-matched interface between them.

The authors are grateful for the financial supports of the key project of the Natural Science Foundation of Zhejiang province (Grant No. Z4080347), Qianjiang Talent Program of Zhejiang Province (Grant No. 2009R10072), the CAS/SAFEA International Partnership Program for Creative Research Teams, the aided program for Science and Technology Innovative Research Team of Ningbo Municipality (Grant No. 2009B21005), and Special Foundation of President of the Chinese Academy of Sciences (Grant No. 080421WA01).

[1] J. F. Wager, Science **300**, 1245 (2003).
[2] R. L. Hoffman, B. J. Norris, and J. F. Wager, Appl. Phys. Lett. **82**, 733 (2003).
[3] N. L. Dehuff, E. S. Kettenring, D. Hong, H. Q. Chiang, J. F. Wager, R. L. Hoffman, C.-H. Park, and D. A. Keszler, J. Appl. Phys. **97**, 064505 (2005).
[4] S. Masuda, K. Kitamura, Y. Okumura, S. Miyatake, H. Tabata, and T. Kawai, J. Appl. Phys. **93**, 1624 (2003).
[5] P. F. Carcia, R. S. McLean, M. H. Reilly, and G. Nunes, Appl. Phys. Lett. **82**, 1117 (2003).
[6] L. Wang, M. H. Yoon, G. Lu, Y. Yang, A. Facchetti, and T. J. Marks, Nature Mater. **5**, 893 (2006).
[7] Dhananjay and C. W. Chu, Appl. Phys. Lett. **91**, 132111 (2007).
[8] Dhananjay, S. S. Cheng, C. Y. Yang, C.-W. Ou, Y.-C. Chuang, M. C. Wu, and C.-W. Chu, J. Phys. D: Appl. Phys. **41**, 092006 (2008).
[9] H. Yabuta, M. Sano, K. Abe, T. Aiba, T. Den, H. Kumomi, K. Nomura, T. Kamiya, and H. Hosono, Appl. Phys. Lett. **89**, 112123 (2006).
[10] H. Odaka, Y. Shigesato, T. Murakami, and S. Iwata, Jpn. J. Appl. Phys. **40**, 3231 (2001).
[11] P. D. C. King, T. D. Veal, F. Fuchs, Ch. Y. Wang, D. J. Payne, A. Bourlange, H. Zhang, G. R. Bell, V. Cimalla, O. Ambacher, R. G. Egdell, F. Bechstedt, and C. F. McConville, Phys. Rev. B **79**, 205211 (2009).
[12] S. Q. Zhang and R. F. Xiao, J. Appl. Phys. **83**, 3842 (1998).
[13] J. Robertson, Eur. Phys. J.: Appl. Phys. **28**, 265 (2004).
[14] M. Gurvitch, L. Manchanda, and J. M. Gibson, Appl. Phys. Lett. **51**, 919 (1987).
[15] L. Manchanda and M. Gurvitch, IEEE Electron Device Lett. **9**, 180 (1988).
[16] Y. J. Cho, J. H. Shin, S. M. Bobade, Y.-B. Kim, and D.-K. Choi, Thin Solid Films **517**, 4115 (2009).
[17] It is assumed that the vacuum levels of the Y_2O_3 and In_2O_3 layer are continuous. Electron affinity energies of Y_2O_3 and In_2O_3 are cited to be 1.7 eV and 4.3 eV, respectively. Hence, it can be shown that the conduction band offset (ΔE_C) of the Y_2O_3/In_2O_3 interface are roughly equal to 2.6 eV.
[18] The IZO electrode materials were deposited by rf magnetron co-sputtering in pure Ar ambient applying a ZnO target and a In_2O_3 target with powers of 100 W and 70 W, respectively. The resistivity of the fabricated IZO films is around 5×10^{-3} Ω cm.
[19] X. J. Wang, L. D. Zhang, J. P. Zhang, G. He, M. Liu, and L. Q. Zhu, Mater. Lett. **62**, 4235 (2008).
[20] P. de Rouffignac, J. S. Park, and R. G. Gordon, Chem. Mater. **17**, 4808 (2005).
[21] M. Harris, H. A. Macleod, S. Ogura, E. Pelletier, and B. Vidal, Thin Solid Films **57**, 173 (1979).
[22] *Handbook of X-ray Photoelectron Spectroscopy*, edited by J. Chastain (Perkin-Elmer, Eden Prairie, MN, 1992).
[23] G. M. Ingo and G. Marletta, Nucl. Instrum. Methods Phys. Res. B **116**, 440 (1996).
[24] J. P. Duraud, F. Jollet, N. Thromat, M. Gautier, P. Maire, C. L. Gressus, and E. Dartyge, J. Am. Ceram. Soc. **73**, 2467 (1990).
[25] R. B. M. Cross, M. M. De Souza, S. C. Deane, and N. D. Young, IEEE Trans. Electron Devices **55**, 1109 (2008).

Downloaded 26 Sep 2010 to 130.237.29.138. Redistribution subject to AIP license or copyright; see http://apl.aip.org/about/rights_and_permissions